Scaling of characteristic frequencies of organic electronic ratchets

Scaling of characteristic frequencies of organic electronic ratchets

Erik M. Roeling,[1] Wijnand Chr. Germs,[1] Barry Smalbrugge,[2] Erik Jan Geluk,[2] Tjibbe de Vries,[2] René A. J. Janssen,[1] and Martijn Kemerink[1,*]

[1]*Applied Physics, Eindhoven University of Technology, PO Box 513, Eindhoven, The Netherlands*

[2]*COBRA Research Institute, Eindhoven University of Technology, PO Box 513, Eindhoven, The Netherlands*

(Received 22 August 2011; revised manuscript received 4 January 2012; published 19 January 2012)

The scaling of the characteristic frequencies of electronic ratchets operating in a flashing mode is investigated by measurements and numerical simulations. The ratchets are based on organic field effect transistors operated in accumulation mode. Oscillating potentials applied to asymmetrically spaced interdigitated finger electrodes embedded in the gate dielectric create a time-dependent, spatially asymmetric perturbation of the transistor channel potential. As a result, a net dc current can flow between source and drain despite zero source-drain bias. The frequency at current maximum is linearly dependent on the charge carrier density and the charge carrier mobility and inversely proportional to the squared length of the ratchet period, which can be related to the RC time of one asymmetric unit. Counterintuitively, it is independent of driving amplitude. Furthermore, the frequency at current maximum depends on the asymmetry of the ratchet potential, whereas the frequency of maximum charge pumping efficiency does not.

DOI: 10.1103/PhysRevB.85.045430 PACS number(s): 73.40.Ei, 73.50.Fq, 73.61.Ph

I. INTRODUCTION

Taming the random motion of particles has drawn scientific interest for over a century.[1,2] The second law of thermodynamics forbids the extraction of work from a system in thermal equilibrium. However, the random motion of particles can be rectified by subjecting the particles to ratchet potentials in systems that are taken out of thermal equilibrium. These potentials consist of repeating units that lack inversion symmetry. The mechanism behind the flashing ratchet is depicted in Fig. 1(a). Particles are trapped in an asymmetric potential. When the potential is turned off, the particles will spread due to diffusion and, in the case of charged particles, due to drift resulting from the interparticle interaction. If the potential is turned on again, particles will get trapped in the energy nearest potential minimum. This is not necessarily the spatially nearest potential minimum. Hence, due to the asymmetry of the repeat unit, a net transport of particles into one direction can result from a driving force that itself has a zero mean. Moreover, this transport can be (partially) based on thermal motion. Both experiments and theoretical work have shown that ratchet systems are complicated systems and show intriguing nonlinear effects like current reversals in response to minute changes in the system.[1,2]

Prominent examples of ratchets are the electronic ratchets, which so far have been of limited use due to cryogenic operating temperatures and low output currents and voltages.[3–7] Recently, we reported on electronic ratchet systems that operate at room temperature and generate currents ($\sim$0.9 μA) and voltages ($\sim$8 V) that are orders of magnitude higher than previously reported systems.[8] Being also effective charge pumps with reported charge displacement efficiencies up to 13%, these systems might lead to interesting applications of electronic ratchet systems.[8,9] Another major advantage of these devices is the good experimental accessibility of a large number of parameters, which enables their in-depth study. In this paper, we describe how the characteristic frequencies of the ratchet, i.e. the driving frequencies yielding the maximum dc current and the maximum charge pumping efficiency, scale with device parameters such as the shape and size of the ratchet potential and the charge carrier density and mobility. We do so by combining experimental and modeling results. So far, the driving frequency dependence of the response of electronic ratchets has hardly been studied experimentally. In this paper, the scaling of characteristic frequencies of (organic) electronic ratchets is investigated by measurements and numerical simulations.

The ratchets studied in this paper consist of bottom-contact, bottom-gate pentacene-based organic field effect transistors (OFETs). Inside the silicon dioxide (SiO_2) gate, dielectric asymmetrically spaced interdigitated finger electrodes, denoted by AF_1 and AF_2 [Fig. 1(b)], are placed. The width of these electrodes is 1 μm. By placing time-alternating potentials on the finger electrodes, according to $V_{AF_1}(t) = V_O + (V_A/2)[1 + \sin(\omega t)]$ and $V_{AF_2}(t) = V_O + (V_A/2)[1 + \sin(\omega t)]$, the principle of the flashing ratchet is mimicked. As a result, a dc current can be induced between the source (S) and drain (D) contacts despite zero bias ($V_{SD} = 0$ V) between the two contacts.[8] Here, V_O is a central offset voltage and V_A is the peak-to-peak voltage of each signal, both set with respect to the grounded source contact. Here, ω is the angular frequency, and t is the time.

Driven as described above, the organic electronic devices depicted in Fig. 1(b) are genuine ratchets, in contrast to simple peristaltic charge pumps, as witnessed by the highly nonlinear dependence of the output current on driving frequency.[1,8] Moreover, their relatively high efficiency was shown to be a collective effect of the distribution of charged particles (holes) in the OFET channel. At least three potentially relevant timescales can therefore be identified, first, the single particle relaxation time τ_{rel}, describing the relaxation of a single hole or electron in the density of states of the semiconductor. Although this time can be up to seconds at low charge densities due to the high degree of disorder in organic semiconductors,[10] the experimental results presented below do not seem to carry any features that are related to this timescale, and in the numerical modeling we shall assume the charge carrier distribution to be

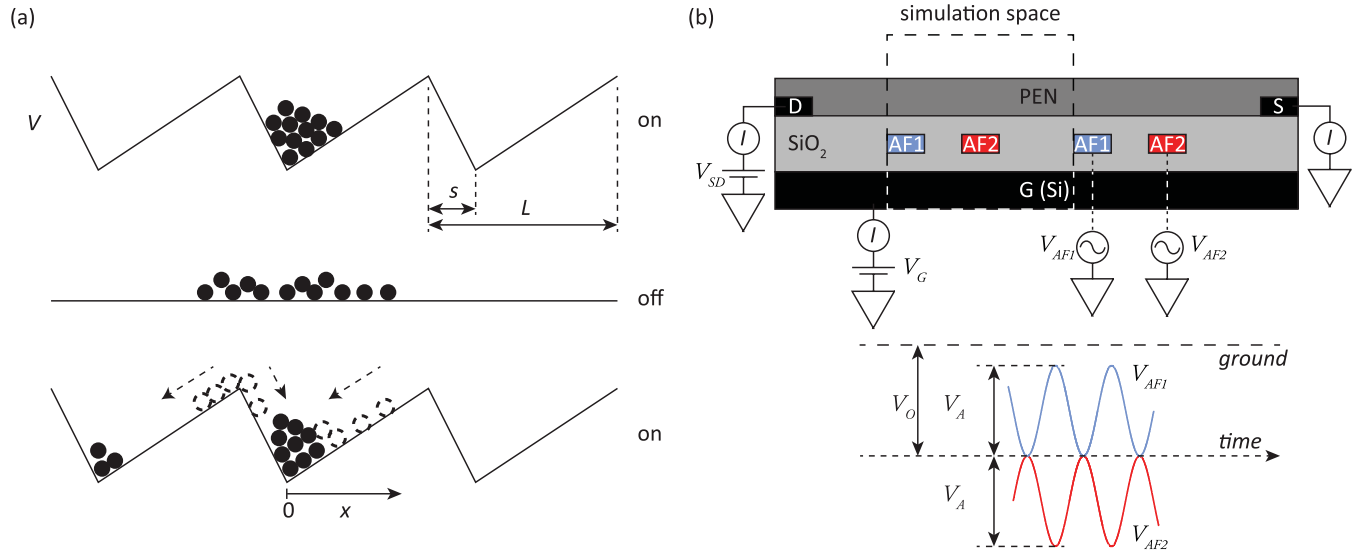

FIG. 1. (Color online) (a) On-off-on sequence of the flashing ratchet. (b) Drawing of an $L1$-$2P2$ ratchet. Visible are the source (S) and drain (D) contacts, which are separated from the silicon (Si) gate (G) contact by the silicon dioxide (SiO_2) gate dielectric. Asymmetrically spaced interdigitated finger electrodes denoted by AF_1 and AF_2 are placed inside the gate dielectric. Note the color coding of the finger electrodes; fingers with the same color are electrically connected (not visible in drawing). Pentacene (PEN) is used as a semiconductor.

always in local thermal equilibrium. The second anticipated timescale is the transit time, i.e. the time a charge carrier needs to travel a characteristic distance L in the device, which for drift-dominated motion is given by

$$\tau_{tr} = L^2/\mu\Delta V \tag{1}$$

with μ the charge carrier mobility and ΔV the electrostatic potential difference across L. For a single particle in a flashing ratchet the optimal on-time was previously found to be $t_{on} = \gamma(1-\alpha)^2L^2/U$, with γ the drag coefficient which is inversely proportional to the mobility μ, $(1-\alpha)$ a constant reflecting the asymmetry of the ratchet and U the barrier height.[11] Apart from these two single-particle timescales, a third timescale related to the collective response can be identified, namely the time the charge carrier distribution needs to globally equilibrate, i.e. to redistribute itself over the entire device after a perturbation. For this, one typically uses the RC time, which for a field effect transistor (FET) is given by

$$\tau_{RC} = L^2/V_G\mu \tag{2}$$

with V_G the gate voltage.[12] Numerical calculations in Ref. 8 show that typical driving frequencies are too fast for the charge distribution to globally equilibrate. In that sense, these electronic ratchets can be considered nonadiabatic. With these constraints, i.e. $f^{-1} \gg \tau_{rel}$ and $f^{-1} \approx \tau_{RC}$, the results presented below are not specific to the particular (organic) material system used and should be general in nature.

On basis of the timescale considerations above, one may anticipate three frequency regimes for the ratchets. At frequencies $f^{-1} \ll \tau_{RC}$, the charge distribution is effectively frozen, yielding zero dc current. Also, at very low frequencies $f^{-1} \gg \tau_{RC}, \tau_{tr}, \tau_{rel}$, a zero dc current is anticipated since the device remains in equilibrium. This paper is concerned with the intermediate regime in which the dc current is anticipated to reach at least one maximum.

The investigated ratchets differ in length and asymmetry, which is reflected in the notation. An Lx-yPa ratchet has an asymmetry of x to y, where x and y are, respectively, the short and long distance in micrometers between the interdigitated finger electrodes AF_1 and AF_2. Here, Pa is the number of pairs of finger electrodes that are present in the device. In some cases, there is a noninteger number of finger electrode pairs, where AF_1 has one finger extra as compared to AF_2 [e.g. Fig. 1(b), showing an $L1$-2P2.5 ratchet]. The L in Lx–yPa stands for length and the P stands for (number of) pairs.

Several parameters might be of influence on the frequency f_I at which maximum dc current is generated, e.g. the gate bias, the amplitude V_A, the asymmetry, the temperature of the system, and the mobility μ of the semiconductor. At high frequencies (10^5–10^7 Hz), the interesting region for maximum current transport, the influence of diffusion on the charge transport is negligible compared to the influence of charge-charge interactions.[8] Therefore, the temperature is not an interesting variable and is kept constant at 40 °C. The offset V_O only affects the current I and not the frequency f_I (not shown). Therefore V_O is kept constant at −7 V. Furthermore, all ratchets are operated in short-circuit mode (i.e. $V_{SD} = 0$ V). In the next sections, first the experimental results will be presented, after which the numerical model will be introduced, and its outcomes will be discussed and compared to experiments.

II. EXPERIMENTAL RESULTS

A. Methods

The ratchets are fabricated on highly p-doped silicon wafers, serving as gate contact. Asymmetrically spaced interdigitated finger electrodes (5-nm Ti/20-nm Au/5-nm Ti) are placed on top of 100-nm thermal SiO_2 by ultraviolet (UV) photolithography. The finger electrodes are 1 μm

wide and 1.5 mm long. They are covered with a 100-nm SiO_2 layer deposited by plasma-enhanced chemical vapor deposition. Subsequently, two 1-mm-long (10-nm Ti/40-nm Au) contacts are positioned symmetrically with respect to the interdigitated fingers on top of the SiO_2 layer, again using UV photolithography. A monolayer of hexamethyldisilazane (HMDS) is applied after which 50-nm pentacene is deposited by thermal evaporation at 0.4 Å/s in a high-vacuum system.

Measurements are conducted at 40 °C in a high-vacuum probe station. Prior to the measurements, the sample is *in situ* heated to 110 °C for over one hour to remove water. A Keithley 4200 parameter analyzer equipped with preamplifiers is used to source voltage and measure current at source, drain, and gate contacts. Both in the experiments and in the modeling discussed in Sec. III, the source Fermi level is used as an energy reference. In the experiments, both the source and drain contacts are always placed at zero bias. An Agilent 81150 dual-channel arbitrary waveform generator is used for applying the potentials on AF_1 and AF_2. Because of the hole density-dependent mobility, the turn-on voltage was used as an approximation for the threshold voltage.

B. Experiments

In Fig. 2, a measured current contour plot for an $L1$-$4P4$ ratchet [see Fig. 1(b)] for different frequencies and amplitudes V_A is shown. The white line indicates f_I for the corresponding amplitude values. Although there is some variation with drive amplitude, the frequency for maximum current seems essentially independent of amplitude, except at the lowest amplitudes where experimental noise dominates. With certainty, a scaling with (reciprocal) transit time, according to Eq. (1), can be excluded.

The influence of the gate voltage for an $L1$-$4P8$ ratchet is displayed in Fig. 3. The contour plot in Fig. 3(a) shows the current values for different frequencies and gate voltages; the white line again indicates f_I. It is well known that, in organic

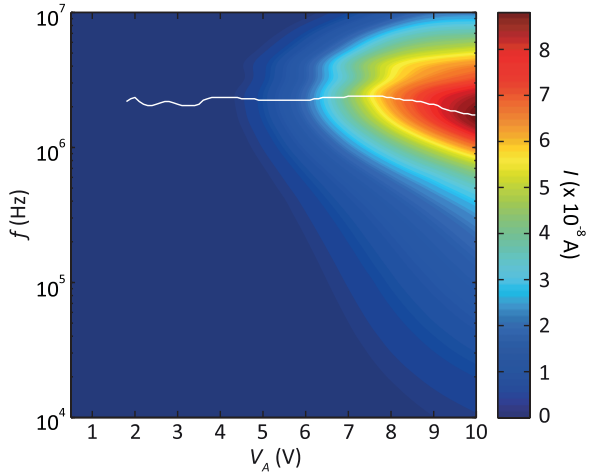

FIG. 2. (Color online) Measured contour plot for an $L1$-$4P4$ ratchet for different frequencies f and amplitudes V_A. The color indicates the ratchet current. The white line shows the frequency at which a maximum current is reached for the corresponding amplitude values. Measurement settings: $V_O = -7$ V, $V_G - V_{TH} = -20$ V, with V_{TH} the threshold voltage.

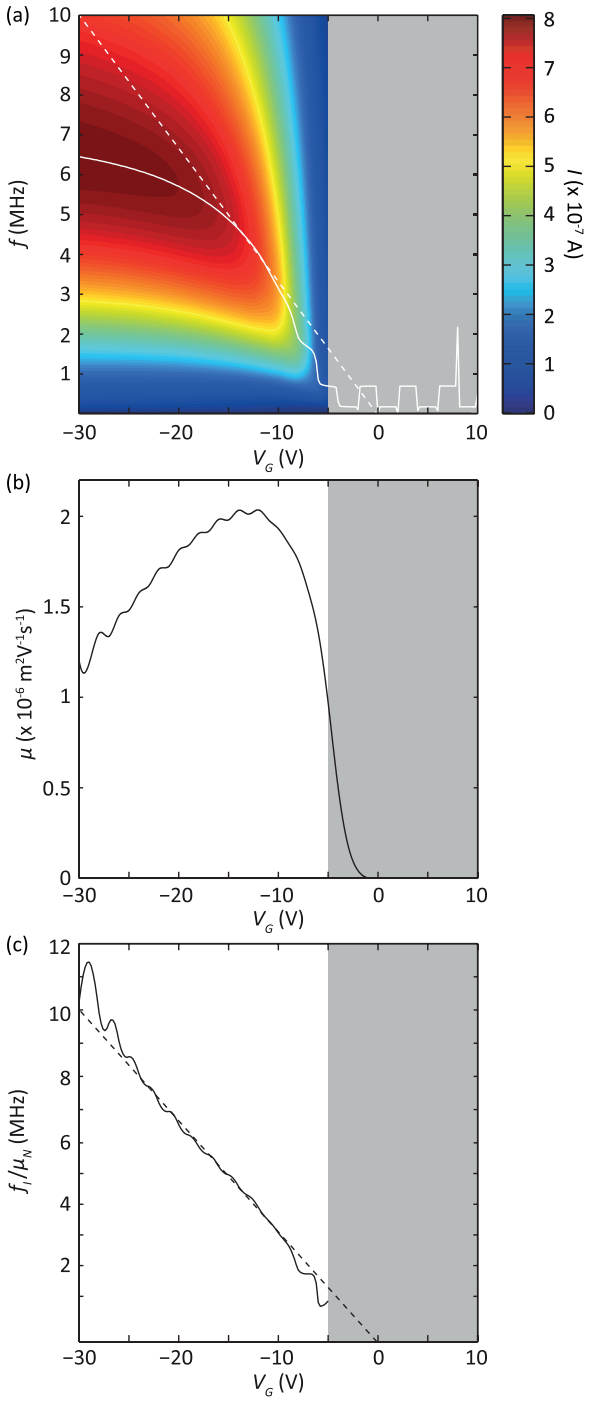

FIG. 3. (Color online) (a) Measured current contour plot for an $L1$-$4P8$ ratchet for different frequencies f and gate voltages V_G. The color indicates the ratchet current I. The white line shows the frequency at which a maximum current is reached for the corresponding gate values. Measurement settings: $V_A = 8$ V, $V_O = -7$ V. (b) Measured mobility μ vs gate voltage V_G for an $L1$-$4P8$ ratchet. (c) Frequency at maximum current f_I of (a) divided by the normalized mobility μ_N of (b) vs the gate voltage V_G. The dashed lines in (a) and (c) show a linear fit to the corrected measurement results in panel (c). The gray areas are the regions where the measured current was below the noise limit.

semiconductors like pentacene, the mobility is density and/or field dependent.[13] As the density depends on the gate voltage,

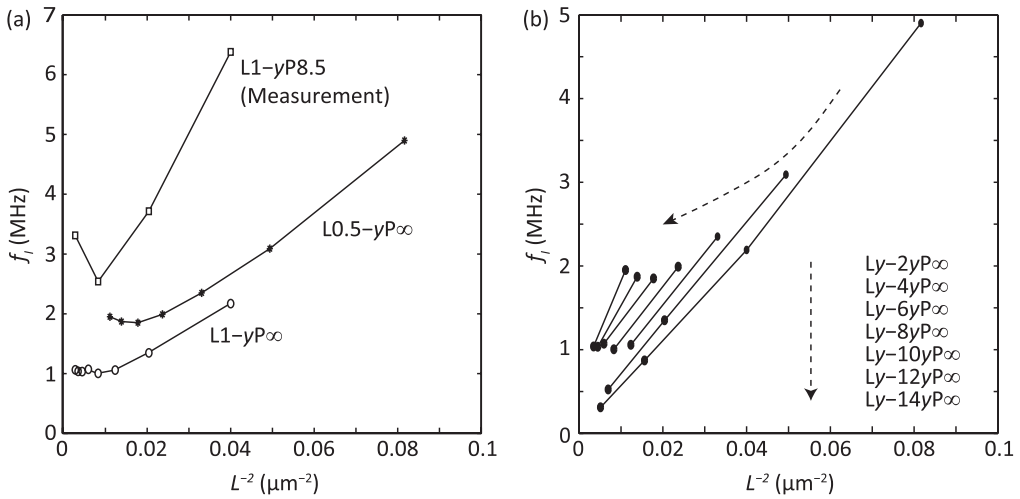

FIG. 4. (a) Measured and modeled frequency at current maximum f_I vs L^{-2} for ratchets with a fixed short distance x of 1 and 0.5 μm (modeling only). (b) Frequency at current maximum f_I vs L^{-2} for ratchets with various, fixed asymmetry ratios. Modeling settings (a): $\mu = 10^{-6}$ m^2/Vs, $V_G = -20$ V, $V_O = -7$ V, $V_A = 8$ V. $L1$-$yP\infty$: y ranges from 2 to 16 μm with steps of 2 μm, $L0.5$-$yP\infty$: y ranges from 1 to 7 μm with steps of 1 μm. Measurement settings (a): $V_O = -6$ V, $V_A = 8$ V, $V_G - V_{TH} = -20$ V. $L1$-$yP\infty$ (measurement): y is 2, 4, 8, and 16 μm. Modeling settings (b): $\mu = 10^{-6}$ m^2/Vs, $V_G = -20$ V, $V_O = -7$ V, $V_A = 8$ V, y values of 0.5, 1, 2, and 4 μm are used.

the data from Fig. 3(a) need to be corrected for this in order to obtain the bare density dependence of f_I—in Sec. III, we will demonstrate that the mobility may indeed be used as a linear scaling factor for f_I. In Fig. 3(b), the measured mobility as a function of the gate voltage is depicted for the $L1$-$4P8$ ratchet. Next, for each gate voltage, the measured frequency at maximum current [panel (a)] is divided by the corresponding normalized mobility μ_N (i.e. $\mu_N(V_G) = \mu(V_G)/\mu_M$, with μ_M the maximum mobility), giving a mostly linear relationship as shown in panel (c). This is a typical result which is found for ratchets with different asymmetries and finger electrode pairs. The wiggles at low gate bias are due to the finite mesh used for V_G and f and the low currents measured. For somewhat larger, i.e. more negative, gate biases, the frequency at maximum current seems to scale with the reciprocal RC time, $f_I \sim \tau_{\mathrm{RC}}^{-1} = V_G\mu/L^2$ [Eq. (2)]. In this expression, it should be noted that the product $V_G\mu$ is proportional to the channel conductivity.

According to Ref. 11, the frequency at current maximum for a single particle flashing ratchet scales with L^{-2}, with L the length of one asymmetric unit. From the introduction, a similar scaling of characteristic frequencies may be anticipated for the organic electronic ratchets as both τ_{tr} and τ_{RC} scale with L^2. In Fig. 4(a), measured frequencies f_I are plotted vs L^{-2} as open squares. The curve suggests that going to larger asymmetries (i.e. smaller L^{-2} values), a minimum in f_I is reached after which a slight increase is observed; a linear scaling with L^{-2} seems absent for the investigated devices. However, a scaling with L^{-2} for devices with constant asymmetry cannot be excluded. In Sec. III (modeling), we will come back to the role of the varying asymmetry in the scaling of f_I.

This section is finished with a brief inspection of the scaling of the frequency at maximum charge per cycle f_Q, instead of at maximum current. Charge per cycle is defined as the cycle-averaged current divided by the drive frequency f. At the frequency f_Q, the charge displacement efficiency (almost) reaches its maximum.[8] The charge displacement efficiency is defined as the net amount of charge moved in one oscillation period over the total amount of moved charge, with moved charge taken as (drift and diffusion) current divided by frequency:

$$\eta_q = \int I_{SD}(t)dt \Big/ \int |I_{SD}(t)|dt \tag{3}$$

where the integrals run over one oscillation cycle. Although physically transparent in its meaning, the charge displacement efficiency is experimentally inaccessible; we therefore use f_Q as an easily accessible approximation. In Fig. 5, f_Q is shown as a function of μ/L^{-2}. Although a monotonic dependency is obtained, a power law fit to the experimental data gives an exponent of -1.4 for the scaling of f_Q/μ with L. Again, in Sec. III, we will come back to the scaling of f_Q with L.

III. MODELING

A. Model description

In the numerical modeling, a single period of an infinitely long device is considered, as indicated by the dashed box in Fig. 1. Hence, no contacts are present. The model works on a 2D rectangular grid on which the device cross section is mapped. For simplicity, the gate and interdigitated fingers are collapsed on a single layer in the calculations. The grid points corresponding to the gate and the interdigitated fingers therefore set a constant and a time-dependent boundary condition, respectively. Moreover, the transport in the accumulation layer, of thickness d ($d \approx 3$ nm), is assumed to be 1D. The left and right hand side of the calculation area are coupled via periodic boundary conditions; hence, an infinitely long device is simulated. A zero vertical electric field is assumed for the top and bottom grid cell layers.

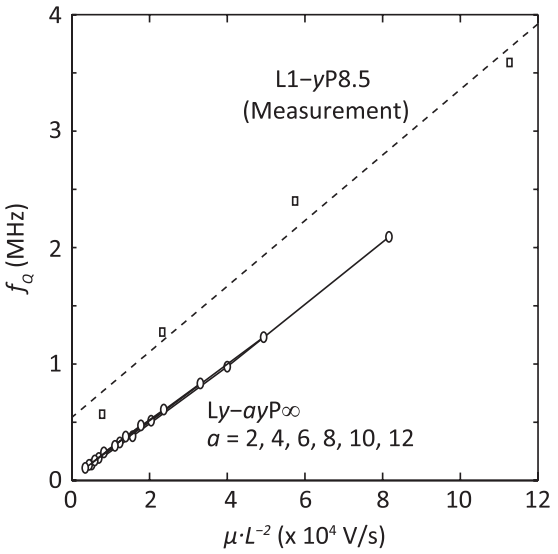

FIG. 5. Measured and modeled frequency at charge maximum f_Q vs μL^{-2} for ratchets with various, fixed asymmetry ratios. The measurement results are obtained for $L1$-$yP8.5$ ratchets with a fixed short distance of 1 μm. The linear dashed line is a guide to the eye. Modeling settings: $\mu = 10^{-6}$ m^2/Vs, $V_G = -20$ V, $V_O = -7$ V, $V_A = 8$ V. Measurement settings: $V_O = -6$ V, $V_A = 8$ V, $V_G - V_{\mathrm{TH}} = -20$ V.

Hole transport is described by the drift-diffusion, continuity, and Poisson equations:

$$j^p = q\mu_p pF - qD_p \nabla p, \tag{4}$$

$$q\frac{\partial p}{\partial t} = -\nabla j^p, \tag{5}$$

$$\nabla(\varepsilon \nabla \phi) = -qp. \tag{6}$$

Here ϕ denotes the electrostatic potential, F the electric field, p the hole concentration, and j^p the hole current density, respectively. Here, D_p and μ_p are the hole diffusion coefficients and mobility, respectively, and are assumed to be connected via the Einstein relation $D = k_B T\mu/q$, where k_B is the Boltzmann constant, T the temperature, and q the elementary charge. Further, $\varepsilon = \varepsilon_0\varepsilon_r$ with ε_0 the permittivity of vacuum and ε_r the relative permittivity.

At time $t = 0$, a fixed amount of charge is placed inside the semiconducting layer. The amount of charge in the accumulation layer is calculated from $p = C(V_{\mathrm{th}} - V_g)/d$ with C the areal gate capacitance and V_{th} the threshold voltage that is taken zero in the model. At each grid point, the time-averaged gate bias V_g is used. In subsequent small time steps, currents are calculated from Eq. (4), which, for each time step, give rise to a change in the carrier density according to Eq. (5) and to a new electrostatic potential according to Eq. (6). Steady state is reached when currents and carrier densities, averaged over one oscillation cycle, no longer change. Since displacement currents average out over a complete oscillation cycle they are not considered here.

In the single-particle limit, the drift-diffusion and continuity equations used here are equivalent to the Fokker–Planck equation that is commonly used for uncharged particles.[1] The major difference with the uncharged particle case is the long-range mutual repulsion between particles, holes in this case, that is accounted for via the Poisson equation.

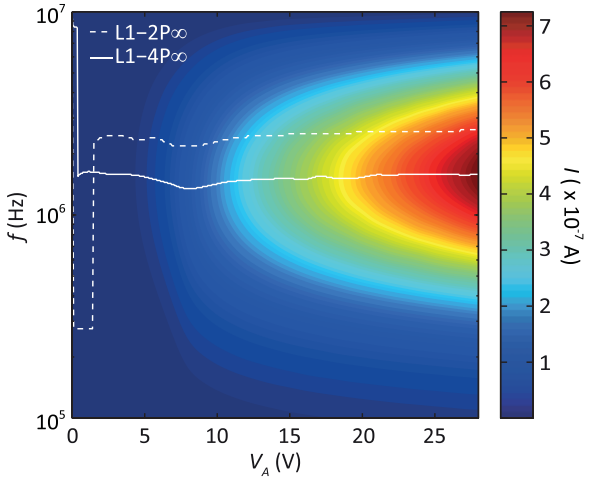

FIG. 6. (Color online) Modeled contour plot for an $L1$-$4P\infty$ ratchet for different frequencies f and amplitudes V_A. The color indicates the ratchet current I. The white lines show the frequencies at which a maximum current is reached for the corresponding amplitude values for an $L1$-$2P\infty$ and $L1$-$4P\infty$ ratchet. Modeling settings: $\mu = 10^{-6}$ m^2/Vs, $V_G = -20$ V, $V_O = -7$ V.

B. Modeling results

In Fig. 6, a calculated current contour plot is shown for an $L1$-$4P\infty$ ratchet for different frequencies f ($f = \omega/2\pi$) and amplitudes V_A. The white lines show for which frequency f_I a maximum current value is reached at the corresponding amplitude values V_A for an $L1$-$2P\infty$ (dashed line) and an $L1$-$4P\infty$ (solid line) ratchet. Like in the experiments of Fig. 2, the results show that the frequency for optimum current transport is essentially independent of the applied amplitude values. At low amplitudes, the current magnitude approaches the numerical noise. In the classical Brownian ratchet, the amplitude of the asymmetric potential plays a major role in the optimum frequency.[11] In that case, larger fields (i.e. larger amplitudes with fixed length scale) decrease the transit time for a particle, as reflected in Eq. (1). Concomitantly, the optimum frequency increases with amplitude. Apparently, the single-particle transit time is not relevant in the electronic ratchets investigated here. This observation is in line with the earlier conclusion that the functioning of these ratchets is due to the collective response of the entire charge distribution in the channel to the fluctuating finger potentials.[8]

Modeling is also used to further investigate the seemingly linear relationship between the gate voltage and the frequency at maximum current f_I that was found in Fig. 3(c). In order to arrive at the curve in Fig. 3(c), we scaled the raw data of panel (a) with the gate voltage-dependent mobility in panel (b). In order to (*a posteriori*) justify this scaling, we investigate by modeling the relationship between the frequency at current maximum and the mobility. The results are depicted in Fig. 7(a). A linear dependence is found between f_I and the mobility for the $L1$-$4P\infty$ and $L1$-$2P\infty$ ratchets. This result is not surprising as the Einstein relation is used to couple

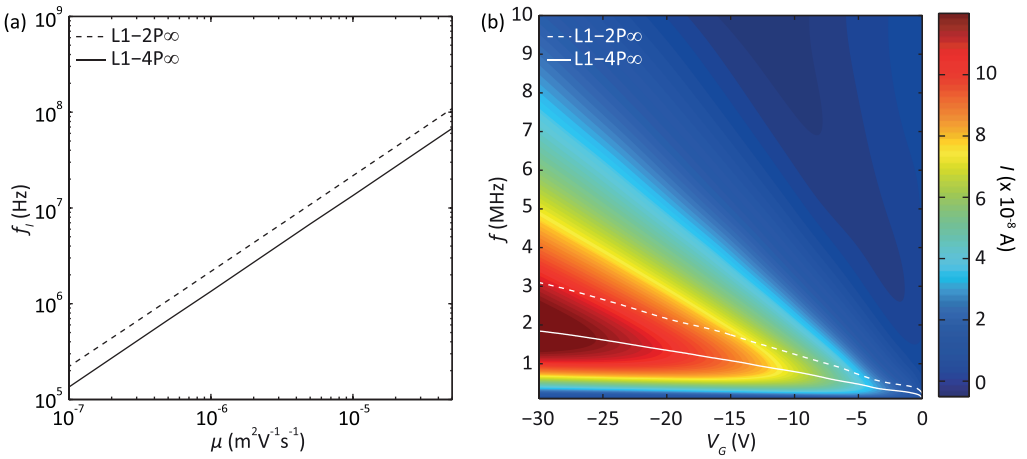

FIG. 7. (Color online) (a) Modeled frequency at current maximum f_I vs mobility μ for an $L1\text{-}2P\infty$ and $L1\text{-}4P\infty$ ratchet. Modeling settings: $V_G = -20$ V, $V_O = -7$ V, $V_A = 8$ V. (b) Modeled contour plot for an $L1\text{-}4P\infty$ ratchet for different frequencies f and gate voltages V_G. Modeling settings: $\mu = 10^{-6}$ m^2/Vs, $V_A = 8$ V, $V_O = -7$ V. The color indicates the ratchet current I. The white lines show the frequency at which a maximum current is reached for the corresponding gate voltage values for an $L1\text{-}2P\infty$ and $L1\text{-}4P\infty$ ratchet.

the diffusion coefficient to the mobility, and hence it can be expected that all transport processes scale linearly with mobility.

The influence of the gate voltage on f_I in the case of a constant, i.e. gate voltage independent, mobility is shown in Fig. 7(b). Like in Fig. 3(c), a linear relation is found. As the charge density in the transistor channel is linearly dependent on the gate voltage, this also implies that the frequency at current maximum is linearly dependent on the charge density.

So far, modeling and measurement results both indicate that $f_I \sim \mu V_G$ and is independent of the driving amplitude V_A. Whether a scaling like Eq. (2) applies for devices of variable repeat unit length but constant asymmetry could not be concluded on the basis of the experiments. In Fig. 4(a), also modeled frequencies f_I are plotted versus L^{-2}. Two ratchet series are modeled; $L1\text{-}yP\infty$ and $L0.5\text{-}yP\infty$ ratchets, where the short distance between two finger electrodes is, respectively, 1 and 0.5 μm. The same trend as observed in the experiments is also visible for the numerically simulated ratchets. The quantitative difference in frequency of maximum current between modeled and measured ratchets is mainly due to differences in mobility. The asymmetry dependence can be removed by investigating ratchets with different periodicity but constant asymmetry. The results for several series of ratchets, where each series has a constant ratio of short and long spacing, are shown in Fig. 4(b). A close to linear relationship is found between the optimum frequency f_I and L^{-2}.

The results presented so far can be summarized by the scaling relation $f_I \sim \mu V_G / L^2 g_{as}$, with g_{as} an unknown function of the asymmetry. Moreover, f_I is independent of driving amplitude V_A. Although the scaling of the frequency at maximum current with key device parameters is hereby largely established, a full quantitative understanding hinges on understanding the origin of g_{as}. It should further be noted that, although f_I scales with reciprocal RC time, it is not equal to that. For instance, in Fig. 6, the reciprocal RC time for the given parameters is 0.8×10^6 and 0.5×10^6 Hz for the $L1\text{-}2P\infty$ and $L1\text{-}4P\infty$ ratchets, whereas f_I is roughly a factor three higher.

Finally, we come back to the scaling of the frequency at maximum charge per cycle f_Q, instead of at maximum current. The modeling results in Fig. 5 indicate that f_Q is proportional to L^{-2} for infinite devices. Surprisingly, unlike f_I, the scaling of f_Q with L^{-2} not only holds for devices with a constant asymmetry but does so for all (modeled) asymmetries: the numerical data points all coincide on a single curve, indicating that f_Q is not influenced by the asymmetry of the ratchet potential. Another difference between the scaling properties of f_Q and f_I is the fact that f_I does [Fig. 3(c)] and f_Q does not scale with V_G. Modeling results for f_Q show significant deviations from a linear scaling with V_G (not shown). The causes underlying these intriguing differences are presently unclear.

IV. SUMMARY

The organic electronic ratchets presented in this paper work by the grace of charge-charge interactions and behave fundamentally different from single-particle ratchets. This is, amongst others, reflected in the different scaling of the characteristic frequencies with operational and geometrical parameters. In the interesting regime for current transport (10^5–10^7 Hz, where diffusion is negligible), modeling and measurement results show that the oscillation amplitude of the driving ratchet potential has a negligible influence on the frequency f_I at which maximum current is reached. This is in stark contrast with single-particle systems reported previously, where the frequency at current maximum was linearly dependent on the amplitude.[11] The importance of collective motion in the present electronic ratchets is further reflected in the (linear) scaling of f_I with the particle density that is set by the gate voltage V_G. As anticipated, the characteristic timescales are linearly related to the charge carrier mobility μ. These findings can be summarized in the scaling relation $f_I \sim \mu V_G / L^2 g_{as}$. The right-hand side of this

relation is, apart from the asymmetry term g_{as}, the reciprocal RC time for one asymmetric ratchet unit. In marked contrast, the frequency at maximum charge transport efficiency does not depend on the asymmetry of the ratchet and scales as $f_Q \sim \mu/L^2$.

Apart from their fundamental interest, the presented scaling rules allow the prediction of the optimum frequency for charge and current transport for electronic ratchets. This can contribute to the rational design of ratchets for use in actual applications.

*Dr. Martijn Kemerink, Dept. of Applied Physics, Eindhoven University of Technology, P.O. Box 513, 5600 MB Eindhoven, Netherlands; m.kemerink@tue.nl

[1]P. Hänggi and F. Marchesoni, Rev. Mod. Phys. **81**, 387 (2009).
[2]P. Reimann, Phys. Rep.: Review Section of Physics Letters **361**, 57 (2002).
[3]H. Linke, T. E. Humphrey, A. Löfgren, A. O. Sushkov, R. Newbury, R. P. Taylor, and P. Omling, Science **286**, 2314 (1999).
[4]V. S. Khrapai, S. Ludwig, J. P. Kotthaus, H. P. Tranitz, and W. Wegscheider, Phys. Rev. Lett. **97**, 176803 (2006).
[5]J. B. Majer, J. Peguiron, M. Grifoni, M. Tusveld, and J. E. Mooij, Phys. Rev. Lett. **90**, 056802, (2003).
[6]S. Sassine, Yu. Krupko, J. C. Portal, Z. D. Kvon, R. Murali, K. P. Martin, G. Hill, and A. D. Wieck, Phys. Rev. B **78**, 045431 (2008).
[7]P. Olbrich, J. Karch, E. L. Ivchenko, J. Kamann, B. März, M. Fehrenbacher, D. Weiss, and S. D. Ganichev, Phys. Rev. B **83**, 165320 (2011).
[8]E. M. Roeling, W. Chr. Germs, B. Smalbrugge, E. J. Geluk, T. de Vries, R. A. J. Janssen, and M. Kemerink, Nat. Mater. **10**, 51 (2011).
[9]P. Hänggi, Nat. Mater. **10**, 6 (2011).
[10]W. Chr. Germs, J. J. M. van der Holst, S. L. M. van Mensfoort, P. A. Bobbert, and R. Coehoorn, Phys. Rev. B **84**, 165210 (2011).
[11]H. Linke, M. T. Downton, and M. J. Zuckermann, Chaos **15**, 026111 (2005).
[12]S. Scheinert and G. Paasch, Phys. Status Solidi A **201**, 1263 (2004).
[13]R. Coehoorn, W. F. Pasveer, P. A. Bobbert, and M. A. J. Michels, Phys. Rev. B **72**, 155206 (2005).